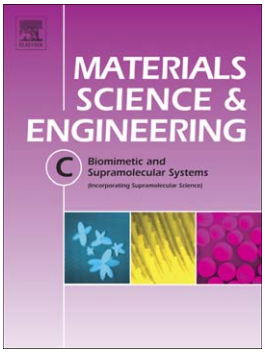

Bioactivity and cell proliferation in radiopaque gel-derived CaO - P_2O_5 - SiO_2 - ZrO_2 glass and glass-ceramic powders

Maziar Montazerian, Bijan Eftekhari Yekta, Vahak Kaspari Marghussian, Caroline Faria Bellani, Renato Luiz Siqueira, Edgar Dutra Zanotto

PII: S0928-4931(15)30114-4
DOI: doi: 10.1016/j.msec.2015.05.065
Reference: MSC 5500

To appear in: *Materials Science & Engineering C*

Received date: 9 January 2015
Revised date: 16 May 2015
Accepted date: 25 May 2015

Please cite this article as: Maziar Montazerian, Bijan Eftekhari Yekta, Vahak Kaspari Marghussian, Caroline Faria Bellani, Renato Luiz Siqueira, Edgar Dutra Zanotto, Bioactivity and cell proliferation in radiopaque gel-derived CaO - P_2O_5 - SiO_2 - ZrO_2 glass and glass-ceramic powders, *Materials Science & Engineering C* (2015), doi: 10.1016/j.msec.2015.05.065

Bioactivity and cell proliferation in radiopaque gel-derived $CaO-P_2O_5-SiO_2-ZrO_2$ glass and glass-ceramic powders

Maziar Montazerian[a,*], Bijan Eftekhari Yekta[a], Vahak Kaspari Marghussian[a], Caroline Faria Bellani[b], Renato Luiz Siqueira[c], Edgar Dutra Zanotto[c]

[a] School of Metallurgy and Materials Engineering, Iran University of Science and Technology, Tehran, 1684613114, Iran

[b] Department of Bioengineering, School of Engineering of São Carlos, University of São Paulo, São Carlos, SP, 13.566-590, Brazil

[c] Department of Materials Engineering, Center for Research, Technology and Education in Vitreous Materials, Federal University of São Carlos, São Carlos, SP, 13.565-905, Brazil

[*]Corresponding author: Maziar Montazerian

Tel.: +98-912-6760071

Fax: +98-21-44065610

E-mail: maziar_montaz@yahoo.com

Abstract

In this study, 10 mol% ZrO_2 was added to a $27CaO-5P_2O_5-68SiO_2$ (mol%) base composition synthesized via a simple sol-gel method. This composition is similar to that of a frequently investigated bioactive gel-glass. The effects of ZrO_2 on the *in vitro* bioactivity and MG-63 cell proliferation of the glass and its derivative polycrystalline (glass-ceramic) powder were investigated. The samples were characterized using thermo-gravimetric and differential thermal analysis (TG/DTA), X-ray diffraction (XRD), Fourier transform infrared spectroscopy (FTIR), and scanning electron microscopy (SEM) coupled to energy dispersive X-ray spectroscopy (EDS). Release of Si, Ca, P and Zr into simulated body fluid (SBF) was determined by inductively coupled plasma (ICP). Upon heat treatment at 1000 °C, the glass powder crystallized into an apatite-wollastonite-zirconia glass-ceramic powder. Hydroxycarbonate apatite (HCA) formation on the surface of the glass and glass-ceramic particles containing ZrO_2 was

confirmed by FTIR and SEM. Addition of ZrO_2 to the base glass composition decreased the rate of HCA formation *in vitro* from one day to three days, and hence, ZrO_2 could be employed to control the rate of apatite formation. However, the rate of HCA formation on the glass-ceramic powder containing ZrO_2 crystal was equal to that in the base glassy powder. Tests with a cultured human osteoblast-like MG-63 cells revealed that the glass and glass-ceramic materials stimulated cell proliferation, indicating that they are biocompatible and are not cytotoxic *in vitro*. Moreover, zirconia clearly increased osteoblast proliferation over that of the Zr-free samples. This increase is likely associated with the lower solubility of these samples and, consequently, a smaller variation in the media pH. Despite the low solubility of these materials, bioactivity was maintained, indicating that these glassy and polycrystalline powders are potential candidates for bone graft substitutes and bone cements with the special feature of radiopacity.

Keywords: Sol-gel; bioactivity; glass; glass-ceramic; zirconia; cell proliferation

Highlights

- A simple sol-gel route was used to synthesize a bioactive $CaO{-}P_2O_5{-}SiO_2{-}ZrO_2$ glass.
- By heat treatment, the glass converted to apatite-wollastonite-zirconia materials.
- HCA formed more rapidly on the crystalline powder surface than on the glass.
- The synthesized powders are bioactive and encourage bone cell proliferation.
- These powders are potential candidates for radiopaque bone grafts and bone cements.

1. Introduction

Sol-gel derived bioactive glasses were first introduced in 1991 in a doctoral dissertation by Li under the supervision of Prof. Larry L. Hench [1]. They demonstrated that the sol-gel process offers great versatility for development of bioactive glasses, i.e., nanoporous powders and even small monoliths [2-4]. In principle, sol-gel derived glass powders can offer higher purity and greater homogeneity than melt-derived powders, and due to their high surface areas, they exhibit much broader ranges of bioactive compositions than glass powders prepared via the melting-quenching route [4,5]. Furthermore, through a controlled heat treatment of a gel-derived glass, a powder or monolith may result. An internally nucleated monolithic sample or a sinter/crystallized glass powder compact can be called glass-ceramics. In the latter case, each particle of the glass-ceramic powder is a conglomerated piece of many individual finer particles, which have been crystallized from their surfaces. For this flexibility of the sol-gel process, numerous attempts have been made to use this process for development of glasses and glass-ceramics for use as bone grafts, scaffolds, coatings and hybrid materials [6-10].

Since its development, the original bioactive gel-glass composition has been modified by numerous scientists. For instance, bioactive glasses containing Mg, Zn, Ag, Sr, Na, K, B, F, Ce, Ga and Sm have been tested, and certain of these materials have special properties for use in specific applications [11-26]. In this work, we focus on the effect of zirconium (Zr) incorporated in the bioactive gel-derived glass powder. In general, Zr can be added to glassy or polycrystalline powders for at least three different purposes: i) to develop radiopaque bioactive powders, and such powders could be mixed with bone cements or bone fillers to improve contrast during radiographic follow up [27]; ii) to develop inert and durable glasses or glass-ceramics for dental restoration build-up on a zirconia core (IPS Cosmo® is a commercial example) [28,29]; and iii) to reinforce bioactive glasses or glass-ceramics [30-36].

Zirconia containing glasses and glass-ceramics have been a field of active research for more than 20 years [27-36]. Normally, these materials have been developed by the well-known sintering or melting-quenching routes, which suffer from certain limitations, e.g., in the course of melting-quenching, zirconia addition often results in an increased melting temperature and

viscosity of the liquid [29-31]. In the sintering route, zirconia powder can be mixed with a glass frit, and the pressed mixture must be sintered and crystallized. However, in this case, zirconia tends to agglomerate during mixing and also increases the sintering temperature. Zirconia dissolution in the matrix and zircon ($ZrSiO_4$) formation represent other drawbacks because they reduce the role of zirconia as reinforcing particles [32-36]. It has been reported that tetragonal zirconia normally confers beneficial effects in improving mechanical properties of ceramic materials due to crack-bending and transformation-toughening mechanisms. Hence, investigators usually prefer to disperse zirconia in the matrix rather than zircon. This strategy has been widely reported in the literature [28-36].

In recent years, the sol-gel process has been used as an alternative route to incorporate zirconium in bioactive glass compositions. It appears that zirconium incorporation into a glass matrix can be performed via sol-gel methods at room temperature, thus avoiding high melting and sintering temperatures. In 2011, the development of Zr-containing mesoporous bioactive scaffolds prepared by a sol-gel method was reported by Zhu *et al.* [37] for the first time. These researchers replaced up to 15 mol% zirconium for calcium in a glass containing $80SiO_2{-}15CaO{-}5P_2O_5$ (molar ratio). Scaffolds were prepared via the combination of a polyurethane sponge and P123 surfactant with a evaporation-induced self-assembly (EISA) process using tetraethoxysilane (TEOS), triethylphosphate (TEP), $Ca(NO_3)_2{\cdot}4H_2O$ and $ZrCl_2$. This study showed that Zr incorporation into the bioactive glass increased the mechanical strength, decreased the chemical solubility, and maintained a more stable pH environment while maintaining the ability to form apatite. Additionally, Persson *et al.* [38] proposed an optimized sol-gel method to produce nano-grain-sized zirconia-silica monolithic glass-ceramics with adequate properties for dental applications and concluded that their material showed promising results for use in dental application; however, the production method is sensitive, and large specimen sizes were difficult to produce. In addition to these two studies, which were intended to develop porous and monolithic Zr-containing bioactive glasses, Ananth *et al.* [39] coated a Ti-6Al-4V alloy with a ZrO_2/bioglass mixture using electrophoretic deposition, and a sol-gel-derived bioactive glass was used in their study. Recently, Tallia *et al.* [40] and Vitale-Brovarone *et al.* [41] developed ZrO_2-containing bioactive mesoporous glass via a sol-gel method. These researchers incorporated zirconium (a radiopaque element) into the structure of a mesoporous

bioactive glass. Radiopacity is an essential feature of bioactive bone cements that allows easy follow-up of the treated patient under radiographic control [27,40,41].

In this study, a simplified sol-gel route using zirconium oxynitrate was employed to produce ZrO_2-containing bioactive $27CaO–5P_2O_5–68SiO_2$ (mol%) glass and polycrystalline powders (glass-ceramic). The main objective was to develop a ZrO_2-containing glass and a glass-ceramic derivative and to compare their *in vitro* bioactivity and biological properties with those of the corresponding ZrO_2-free glass and glass-ceramic. Our goal was to develop and test a bioactive radiopaque powder using a simple sol-gel method. The originality of this work rests on three factors: i) the complete effects of ZrO_2 on this highly studied bioactive glass composition have not yet been investigated; ii) zirconium oxynitrate was applied to introduce ZrO_2 into the glass composition. This new precursor is soluble in the reaction medium and cheaper than the other precursors normally used for this purpose, such as zirconium alkoxides and chlorides; and iii) other researchers have reported the effect of ZrO_2 on the properties of different glass compositions. Here we investigated its effect on *in vitro* bioactivity and cell-proliferation of both glass and derived polycrystalline powders.

2. Materials and methods

2.1. Preparation of gels

The preparation of the gels involved hydrolysis and polycondensation reactions after mixing stoichiometric amounts of tetraethoxysilane (TEOS, $Si(OC_2H_5)_4$), triethylphosphate (TEP, $OP(OC_2H_5)_3$), calcium nitrate tetrahydrate ($Ca(NO_3)_2{\cdot}4H_2O$) and zirconium oxynitrate ($ZrO(NO_3)_2{\cdot}XH_2O$; X ~3) provided by Sigma-Aldrich. This procedure describes a common method used to produce glasses via sol-gel.

The chemical compositions of the base glass and the batch containing zirconium are shown in Table 1. The hydrolysis of TEOS and TEP was catalyzed with a solution of 0.1 $mol.L^{-1}$ HNO_3 using the molar ratio $(HNO_3 + H_2O) / (TEOS + TEP) = 15$. Beginning with the hydrolysis of TEOS, the other reagents were sequentially added at 45-minute intervals, keeping the solution under constant stirring. The sols were poured into Teflon® tubes and stored until gel formation. At the end of this period, which lasted 10 days, the gels were dried for three days at 70 °C and for

one day at 150 °C. After completion of the drying step, the gels were manually crushed in an agate mortar and powders with a particle size < 300 μm were selected and characterized. The base gel and the gel containing zirconium were identified as G and G-Zr, respectively.

Table 1. Nominal composition of glasses with and without zirconium.

Sample		SiO_2	CaO	P_2O_5	ZrO_2
G	mol%	68	27	5	-
	wt.%	64.7	24	11.3	-
G-Zr	mol%	61.2	24.3	4.5	10
	wt.%	53.2	19.7	9.2	17.9

2.2. Conversion of the gels into glass and glass-ceramic powders

Immediately after milling, individual portions of approximately 20 g of the powdered dried gels were placed in alumina crucibles, which were heat-treated in an electric furnace at high temperatures under an oxidizing atmosphere (air). The heating programs were determined using the results of previous differential thermal analyses (DTA) and thermo-gravimetric (TG) analyses of the starting gels. The established thermal treatment programs consisted of heating at 5 °C.min^{-1}, followed by an isothermal heat treatment at 700 °C and 1000 °C to obtain the glass and glass-ceramic powders, respectively. The polycrystalline materials obtained by treatment at 1000 °C were referred to as GC and GC-Zr. The cooling process of the samples in the electric furnace was natural. The names of the samples and heat treatment program are summarized in Table 2.

After completion of the heat treatment, the resulting powders were manually disaggregated in an agate mortar. Powders with particle sizes between 25 μm and 75 μm were selected and submitted to a series of analytical tests.

Table 2. Heat treatment program for conversion of gels into glasses (G) and glass-ceramics (GC).

Sample	Final treatment temperature (°C)	Duration (minutes)
G	700	180
G-Zr	700	180
GC	1000	180
GC-Zr	1000	180

2.3. *In vitro* bioactivity test

To evaluate the bioactivity of the synthesized materials, *in vitro* tests were performed according to the method described by Kokubo *et al.* [42]. The simulated body fluid (SBF) used in this study was acellular and protein-free with a pH of 7.40. Table 3 shows the composition of this solution compared with that of human blood plasma [42].

Table 3. Ionic concentration of human blood plasma and SBF used for evaluation of *in vitro* bioactivity [42].

Simulated Body Fluid (SBF)	**Ionic concentration(mmol.L^{-1})**							
ISO 23317 (June 2007)	Na^+	K^+	Mg^{2+}	Ca^{2+}	Cl^-	HCO_3^-	HPO_4^{2-}	SO_4^{2-}
Human blood plasma	142.0	5.0	1.5	2.5	103.0	27.0	1.0	0.5
***SBF**	142.0	5.0	1.5	2.5	147.8	4.2	1.0	0.5

*Buffer: Tris(hydroxymethyl)aminomethane (TRIS)

2.3.1. Sample preparation

To test the *in vitro* bioactivity of our materials, the previously characterized powders with particle sizes between 25 μm and 75 μm were formed into pellets 10 mm in diameter and ~ 2 mm in height. This forming process consisted of two steps. First, the powders were uniaxially pressed at 65 MPa for 5 minutes and then in an isostatic press at 170 MPa for 3 minutes. Soon after formation, each pellet was fixed along its circumference by a nylon string to allow suspension in the SBF. The samples were first cleaned for 15 s in acetone and after drying were soaked in a polyethylene bottle containing the SBF. The same mass (0.25 g) was used to form the pellets for the all samples. Because the densities of the glass and glass-ceramic were different, the pellets related to the sample with the highest powder density (GC-Zr) were slightly smaller. Therefore, the volume of SBF used in each bioactivity test was calculated according to the geometric area of each type of sample according to the procedure described by Kokubo *et al.* [42]:

$$V_s = S_a / 10 \qquad (1)$$

where V_s represents the volume of the SBF (mL), and S_a represents the total geometric area of the sample (mm^2).

During the test, the samples were kept in contact with the SBF for 3, 6, 12, 24, 48, 72 and 96 h, and the system temperature were maintained at 37 °C. After the time required for testing, each sample was removed from its bottle and immersed in acetone for 10 s for removal of solution and to halt surface reactions. After drying, both sample surfaces were analyzed to check for formation of a superficial HCA layer.

2.3.2. Evaluation of the solubility of samples in SBF

To evaluate the solubility of the samples in SBF during the bioactivity test, the ionic concentrations of calcium, phosphorus, silicon and zirconium were determined by optical emission spectrometry with inductively coupled plasma (ICP-OES) in a Perkin Elmer Optima 7300 instrument for each given testing time. This evaluation was accomplished three times on average for each test time.

2.4. Cell proliferation

For cell culture preparation, human osteoblast-like MG-63 cells were maintained in DMEM medium (Vitrocell®, Embriolife™) supplemented with 10% fetal bovine serum, 1% penicillin, and 1% streptomycin (100 mg/mL) at 37 °C in an atmosphere supplemented with 5% CO_2. Prior to cell seeding, the samples were sterilized under high pressure at 120 ºC for 20 min. For the cell proliferation assay, the cells were trypsinized (trypsinization is the process of cell dissociation using trypsin, a proteolytic enzyme which breaks down proteins to dissociate adherent cells from the vessel in which they are cultured), counted and seeded at 1×10^4 per well in a 24-well TCPS plate. The cell medium was changed every two days.

AlamarBlue® staining (Life Technologies™) was used for cell proliferation assay, which quantitatively measures cell proliferation on several human and animal cell lines, bacteria or fungi. It has many advantages over other cell proliferation tests, e.g., a study has shown that

alamarBlue® gives improved sensitivity and performance when compared to MTT assays [43] and it is not toxic for cells, and has a low cost. Continuous cell growth maintains a reduced environment (fluorescent, red). Inhibition of cell growth maintains an oxidized environment (non-fluorescent, blue) [44]. The cell proliferation assay was performed at 1, 3, 6, 12 and 18 days after cell seeding, in order to understand aspects of ion release from the samples on cells. The results could be useful to further understand *in vivo* analysis because bioactive glasses stay longer into the organism during *in vivo* tests. We used four specimens of each sample per test, and three independent essays. At each point in time, the medium was aspirated, and 600 µL of fresh medium containing 10% of AlamarBlue® (v/v) was applied into each well that contained samples; two empty wells were used as reagent blanks (control of alamarBlue®). The cells were incubated at 37 °C for 4 h. After incubation, 100 µL of medium was transferred into a 96-well TCPS plate, and 100 µL of 100% reduced alamarBlue® (obtained by autoclaving for 15 min) of the cell culture medium with 10% reagent was used as a positive control.

Next, the sample fluorescence was measured at an excitation wavelength of 544 nm and an emission wavelength of 590 nm on a Spectra Max Gemini XS instrument from Molecular Devices™. Finally, cell proliferation was quantified in terms of percentage reduction in alamarBlue®, i.e.:

$$\mathrm{Re}duced\ \ alamarBlue^{®}\,(\%) = \frac{(sample\ value - negative\ control\ value)}{(100\%\ reduced\ \ positive\ control\ value - negative\ control\ value)} \times 100 \qquad (2)$$

2.4.1. Statistical Analysis

Statistical comparisons were performed using two-way ANOVA carried out with GraphPad Prism® software and the Bonferroni multiple comparisons test. P-values < 0.05 were considered statistically significant (n=4).

2.5. Instrumental analysis procedures

2.5.1. Simultaneous thermal analysis (DTA-TG)

Simultaneous thermal analyses (DTA-TG) were performed in a Netzsch STA 409 PC instrument under an oxidizing atmosphere (synthetic air) with a gas flow of 50 mL.min^{-1}. Typical

analysis involved 18 mg of the gel particles and a heating program with a rate of 5 °C.min^{-1} from room temperature to 1100 °C to determine the initial heat treatment temperature and the onset of formation of the crystalline phases.

2.5.2. X-ray diffraction (XRD)

Characterization of the crystalline phases resulting from the heat treatments was performed by XRD. We used a JEOL-JDX-8030 diffractometer operating with CuK_α radiation (λ = 0.15418 nm). The diffraction patterns were obtained in the 2θ range from 10° to 80° in continuous mode at 0.02° min^{-1}. The crystallized volume fraction contained in the polycrystalline samples was estimated using the procedure established by Krimm and Tobolsky [45]. The percent crystallinity (I_C) was estimated using the ratio of the crystalline area (A_C) of the peaks of the X-ray diffractogram of the polycrystals and the total area (A_T = crystalline + amorphous) of the same diffractogram via the following equation:

$$I_C = \left(\frac{A_C}{A_T}\right) \times 10(\qquad (3)$$

2.5.3. Fourier transform infrared spectroscopy (FTIR)

Monitoring of pellet surface modifications after the *in vitro* bioactivity tests was performed via FTIR using a PerkinElmer Spectrum GX model spectrometer operating in reflectance mode with a 4 cm^{-1} resolution in the 4000-400 cm^{-1} region.

2.5.4. Scanning electron microscopy and microanalysis (SEM-EDS)

Morphological characterization of the pellets with respect to surface modifications after the *in vitro* bioactivity test was performed using SEM. A set of samples was selected and analyzed before and after soaking in SBF at different testing times. The samples were coated with a thin gold layer and analyzed under a FEI Magellan 400 L microscope coupled to an energy dispersive X-ray spectroscopic analysis system (EDS), which aided the surface characterization through qualitative chemical analysis.

3. Results and discussion

3.1. Thermal characterization of dried gels

The results of the simultaneous DTA and TG analyses are shown in Figure 1 (a) and (b) for samples G and G-Zr, respectively.

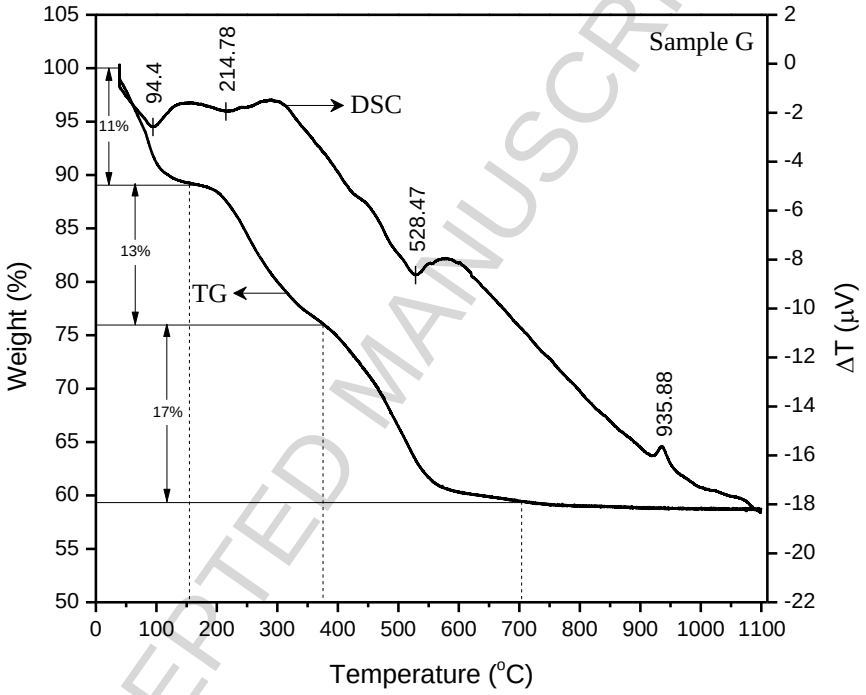

(a)

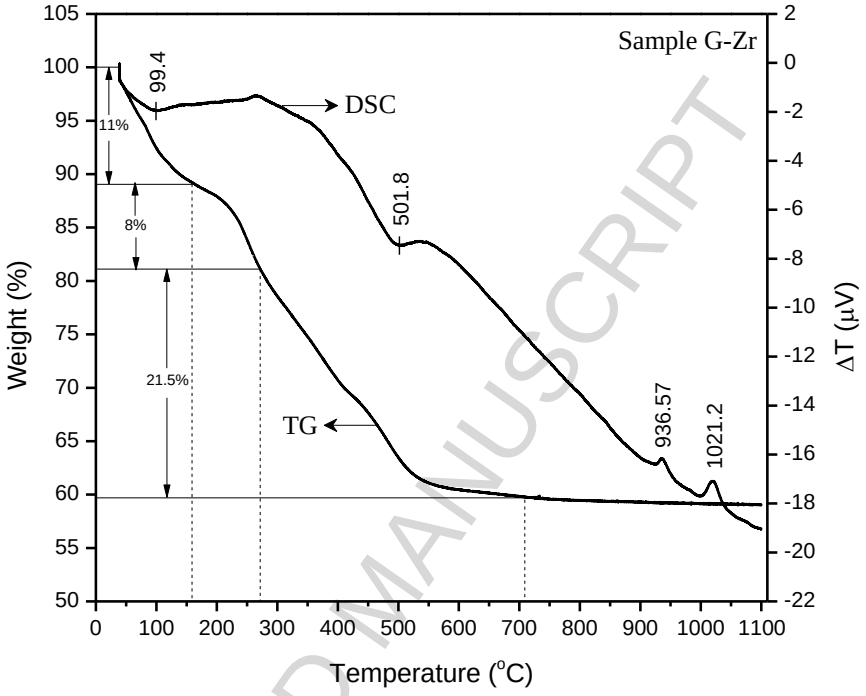

(b)

Figure 1. DTA and TG curves for samples G (a) and G-Zr (b).

These gels undergo three distinct mass loss steps and become virtually stable at approximately 700 °C. The first mass loss step occurs at ~ 25-160 °C and is associated with the endothermic process of desorption of physically adsorbed water and alcohol [13,15,16]. The second mass loss step takes place near 250 °C and is related to the volatilization of water, an endothermic chemical desorption process [12,13]. The third mass loss stage, which can be observed for samples G and G-Zr between 375-702 °C and 271-708 °C, respectively, was more pronounced. This stage is attributed to the evolution of the resulting sub-products from incomplete condensation of the precursors, mostly elimination of the nitrate ions originated from $Ca(NO_3)_2{\cdot}4H_2O$ and $ZrO(NO_3)_2{\cdot}XH_2O$ [12,13]. Further weight loss due to the nitrate decomposition in sample G-Zr could be related to the substitution of zirconium oxynitrate for TEOS and TEP (when Zr-oxynitrate replaces TEOS and TEP, additional weight loss of nitrate is observed). The exothermic peaks located near 935 °C and 1020 °C are associated with the onset of crystallization.

3.2. Conversion of gels into glass and glass-ceramic powders

Based on the DTA and TG analyses, the stabilization temperature used to convert the dried gels to glasses was set to 700 °C. Treatment for 3 h was considered sufficient for complete elimination of the nitrate ions. Furthermore, this condition also indicates the possibility of obtaining glassy materials because crystallization was only observed in a DTA run at ~ 935 °C. To obtain a glass-ceramic, heat treatment at 1000 °C for 3 h was performed. According to the X-ray diffractograms shown in Figure 2, samples G and G-Zr appear to be non-crystalline. However, the diffraction pattern of sample G shows one diffuse reflection centered at 2θ = 32°. This peak is attributed to the presence of apatite [11,46,47]. In the glass-ceramics known as GC and GC-Zr, apatite-wollastonite and apatite-wollastonite-zirconia crystals were formed, respectively.

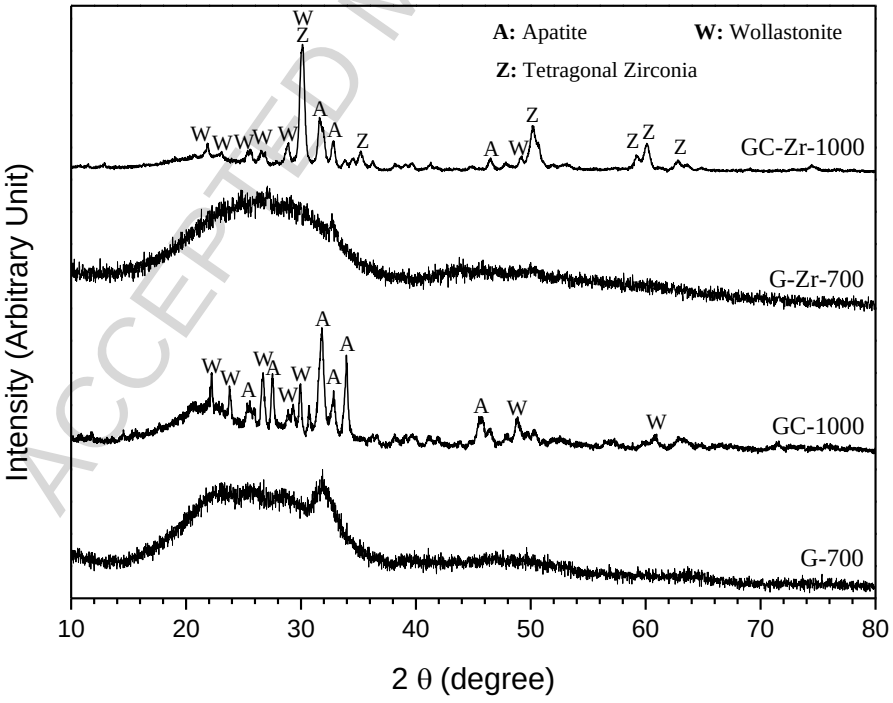

Figure 2. XRD patterns of G and G-Zr glasses and their glass-ceramic derivatives (GC and GC-Zr) heat-treated at 700 °C and 1000 °C, respectively.

Heat treatments above 1000 °C were not considered to avoid zirconia reaction with the matrix components (~ 1100 °C), cristobalite formation (~ 1200 °C) and transformation of wollastonite to pseudo-wollastonite (~ 1300 °C). We avoided treatment at higher temperatures

because various new phases would have appeared in a complicated microstructure. We expected that we could significantly impair bioactivity with the formation of such inert phases and a notably low amount of residual glass.

It has been reported that zirconia has a great tendency to react with the residual glass phases in silicate glasses to form zirconium silicate ($ZrSiO_4$) [29-33]. Wollastonite is soluble and bioactive, but its high temperature polymorph of pseudo-wollastonite is less soluble [48-50]. Cristobalite leads to matrix cracking during cooling and degradation of bioactivity [10,11,48,49]. Finally, it can be concluded that the exothermic peaks observed in Figure 1 at approximately 935 ºC and 1020 ºC can be attributed to the crystallization of apatite and zirconia, respectively.

3.3. *In vitro* bioactivity test

3.3.1. Hydroxycarbonate apatite (HCA) formation

The particle morphologies of glasses G and G-Zr and their respective qualitative chemical analysis before and after exposure to SBF at different testing times are shown in Figure 3. Spherical aggregates can be observed on the surface of samples G and G-Zr after 12 h. These aggregates are similar to primary amorphous calcium phosphate, which begins to form at the fourth stage of the proposed mechanism for hydroxycarbonate apatite (HCA) formation on bioactive glasses [2,51]. Significant superficial changes related to the morphology and chemical composition of the samples could be observed starting from the test times of 24 h and 72 h for samples G and G-Zr, respectively. During this stage, HCA crystallizes and begins to grow. Therefore, the samples submitted to these testing times showed the typical spherical morphology of HCA but still exhibited an amount of space left between the apatite particles (Fig. 3). To verify the behavior of the HCA layer formed at the sample surfaces, a test was performed over 144 h. With such a long testing duration, we observed a more homogeneous HCA layer with larger granules than those formed after 24 and 72 h. According to this morphology, the formation of HCA has already well established with increased test time.

The development of the HCA layer on the surface of these materials was also monitored via EDS. The spectra from sample G in Figure 3 show a large compositional change on the surfaces after 24 h of testing, which was also observed for sample G-Zr after 72 h. Even with

increasing migration of Ca and P to the surface of these samples, the presence of Si is still evident, which can be explained by the low density of the formed HCA layer, thus allowing the detection of the existing Si on the surface immediately below this layer. For samples with 144 h of testing, the presence of Si was minimally observed, whereas the presence of Ca and P became almost exclusive. Thus, it is reasonable to conclude that for 144 h of testing, the samples were completely covered by a HCA layer. Furthermore, Zr addition to the glass increases the time necessary for apatite formation from 24 h to 72 h.

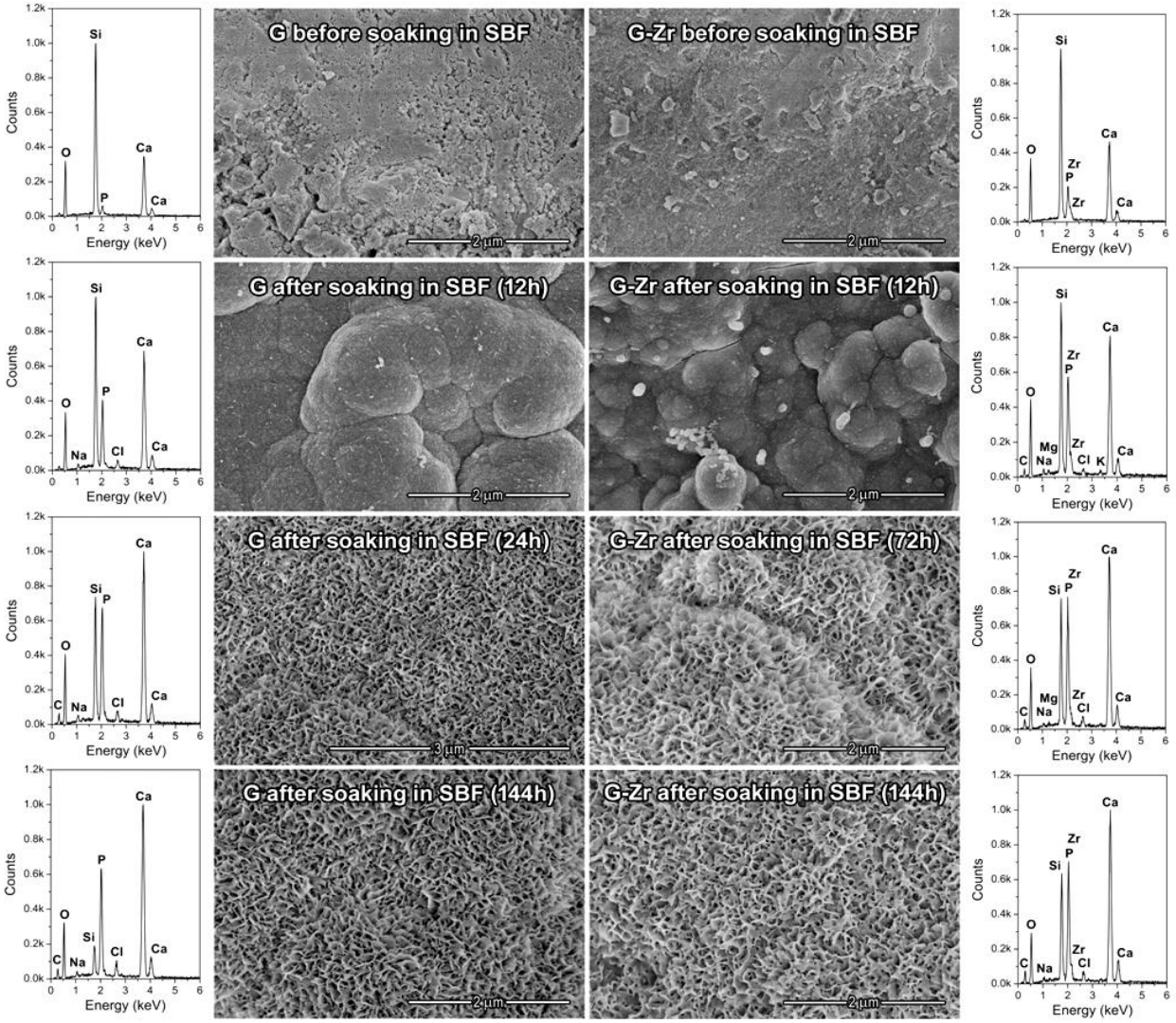

Figure 3. SEM micrographs and EDS spectra of G and G-Zr sample surfaces: Before and after 12 h, 24 h, and 144 h exposure to SBF.

The SEM images of the surfaces of GC and GC-Zr and the corresponding EDS analyses before and after exposure to SBF at different testing times are shown in Figure 4. Formation of fine spherical silica gel particles corresponding to the third stage of the bioactivity mechanism is evident on the surface of the samples after 12 h of exposure to SBF [2,51]. The surface of sample GC was covered by HCA after 24 h. However, in sample GC-Zr, only a thin layer of HCA began to grow for this test time period. For a testing time of 144 h, the surface of the sample GC was fully covered with HCA, similar to the glass sample shown in Figure 3. However, in sample GC-Zr, only the fissures and pores were fully packed with HCA. For this sample, 336 h (14 days) was necessary for HCA to fully cover the surface.

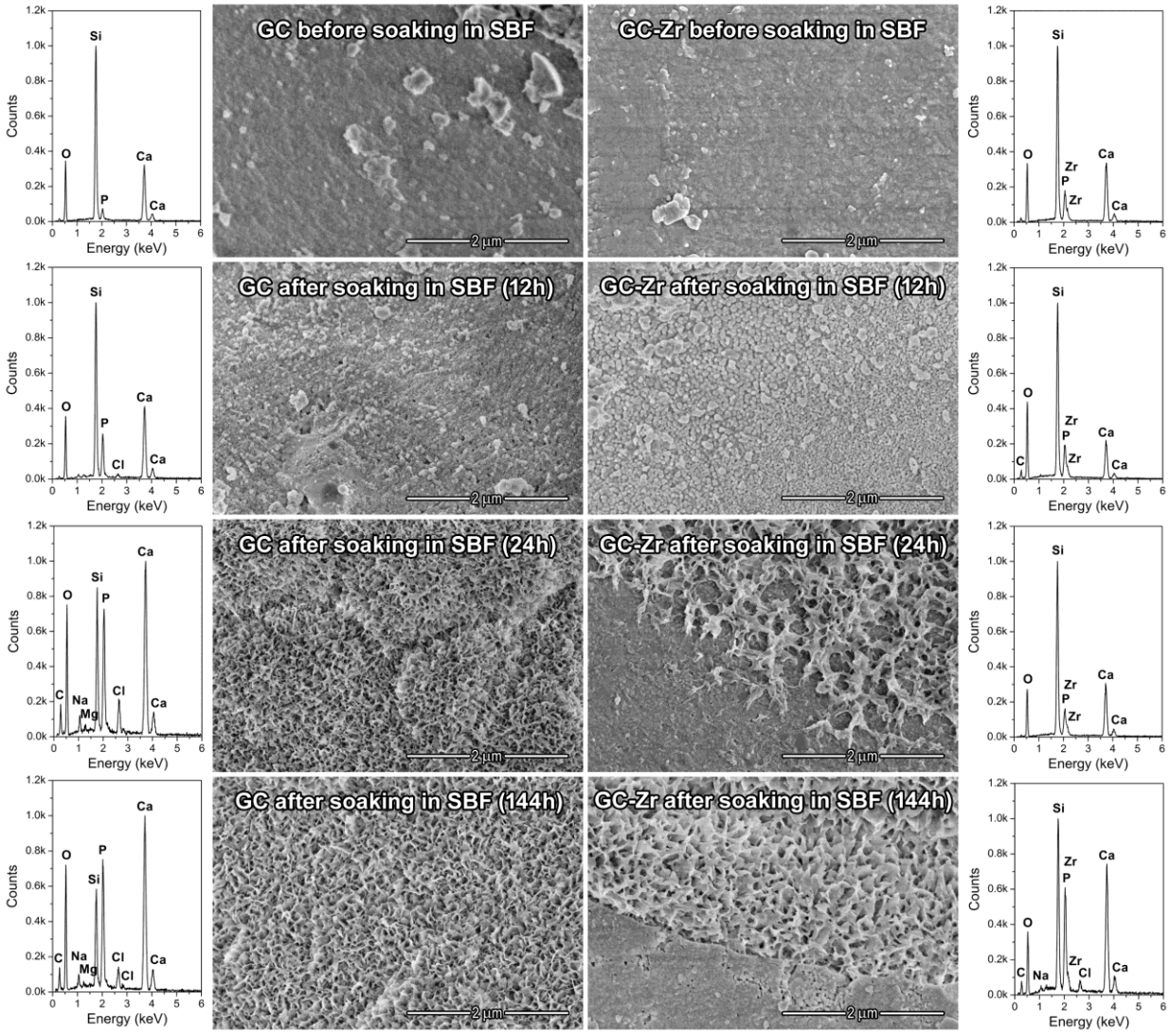

Figure 4. SEM micrographs and EDS spectra of GC and GC-Zr sample surfaces: Before the SBF test and after 12 h, 24 h and 144 h exposure to SBF.

Hence, apatite formation on the surface of the glass-ceramic containing zirconia takes much longer than on the base glass-ceramic. This observation can be partially related to the lower content of residual glass in sample GC-Zr (37% residual glass) than in GC (56% residual glass) and is also due to the presence of Zr ions in the residual glass of the former, which reduces its solubility. It is also interesting to note that the formation of HCA on the surface of the glass-ceramic containing ZrO_2 crystals (GC-Zr) begins sooner than on the ZrO_2-containing glass (G-Zr). In the performed experiments, HCA formed on the surface of sample G-Zr after 72 h, but this process was observed for sample GC-Zr after only 24 h. This observation is likely related to the effect of crystallization and the role of the residual glass composition. Before crystallization, the glass contains zirconium as a dissolved ion, which transforms to zirconia crystals after heat treatment at 1000 °C. Hence, crystallization of this phase depletes the Zr ions in the residual glass. The residual glass, which is now locally depleted in Zr, is rich in P and Ca and is thus likely more soluble than the parent glass.

Figure 5 shows the progressive formation of HCA on the surface of the sample GC-Zr. The fissures are fully packed with HCA after a 144 h exposure to SBF. This observation indicates that fissures and pores are the first locations to become saturated with released P and Ca ions, which makes them favorable locations for HCA nucleation and growth because the Ca and P ions only need to travel a short distance to reach the silica gel previously formed on the surface.

This phenomenon can be easily traced in GC-Zr sample in which HCA forms on the surface over a longer time. Additionally, it is worth noting that the mechanism proposed by Hench for bioactivity can be followed for GC-Zr sample, which demonstrates more controlled release of ions during the testing periods [2,3,46,51].

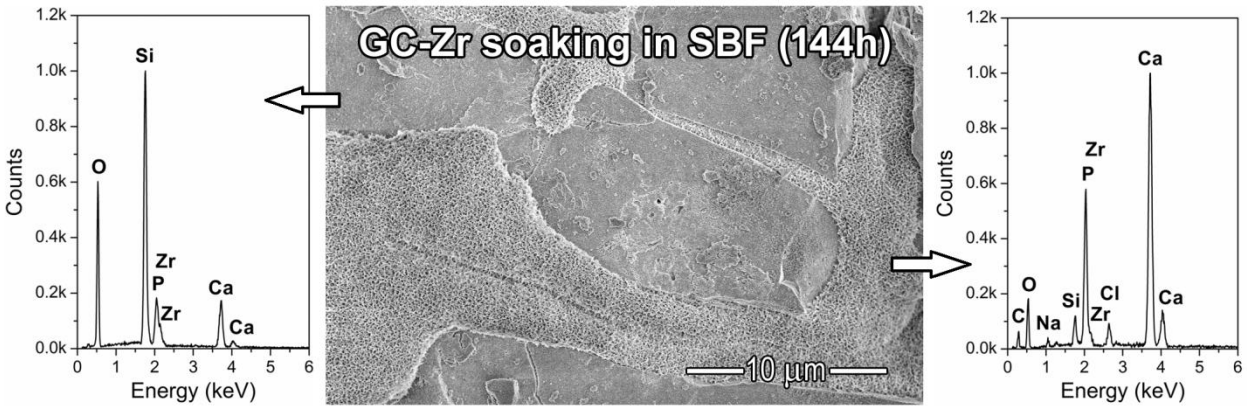

Figure 5. SEM micrograph and EDS spectra from the surface of sample GC-Zr after 144 h exposure to SBF. Hydroxyapatite fills in the fissures and porosities and begins to grow.

The FTIR spectra from the glass and glass-ceramic surfaces before and after exposure to SBF are shown in Figure 6 and 7, respectively. Before the SBF test, glass samples G and G-Zr (Fig. 6 a-b) exhibited two spectra characterized by the presence of bands at approximately 1100 cm^{-1} and 465 cm^{-1}, which are associated with asymmetric stretching vibration and bending vibration of Si–O–Si bonds, respectively [10,12,15]. After 3 h of testing, it is possible to note a broad vibration band at approximately 560 cm^{-1}, which becomes obvious after 12 h and 24 h for samples G and G-Zr, respectively. This change in the spectra can be attributed to stage 4 of the proposed mechanism for bioactivity, which culminates with formation of an amorphous calcium-phosphate-rich layer on the sample surface [2,51]. For a testing time of 24 h for sample G (Fig. 6-a) and 72 h for sample G-Zr (Fig. 6-b), the obtained spectra were similar to the synthetic HCA spectrum, exhibiting changes related to the intensity of the typical HCA bands, located near 1255 cm^{-1}, 1130 cm^{-1}, 1055 cm^{-1}, 605 cm^{-1} and 560 cm^{-1} [3,9,11,12,49]. The observed increase in the intensity and sharpness of these bands after 144 h is associated with the higher density of the formed HCA layer on the sample surfaces. This process also could be monitored in the SEM micrographs and EDS spectra shown in Figure 3, which confirm the formation of HCA in samples G and G-Zr after 24 h and 72 h, respectively.

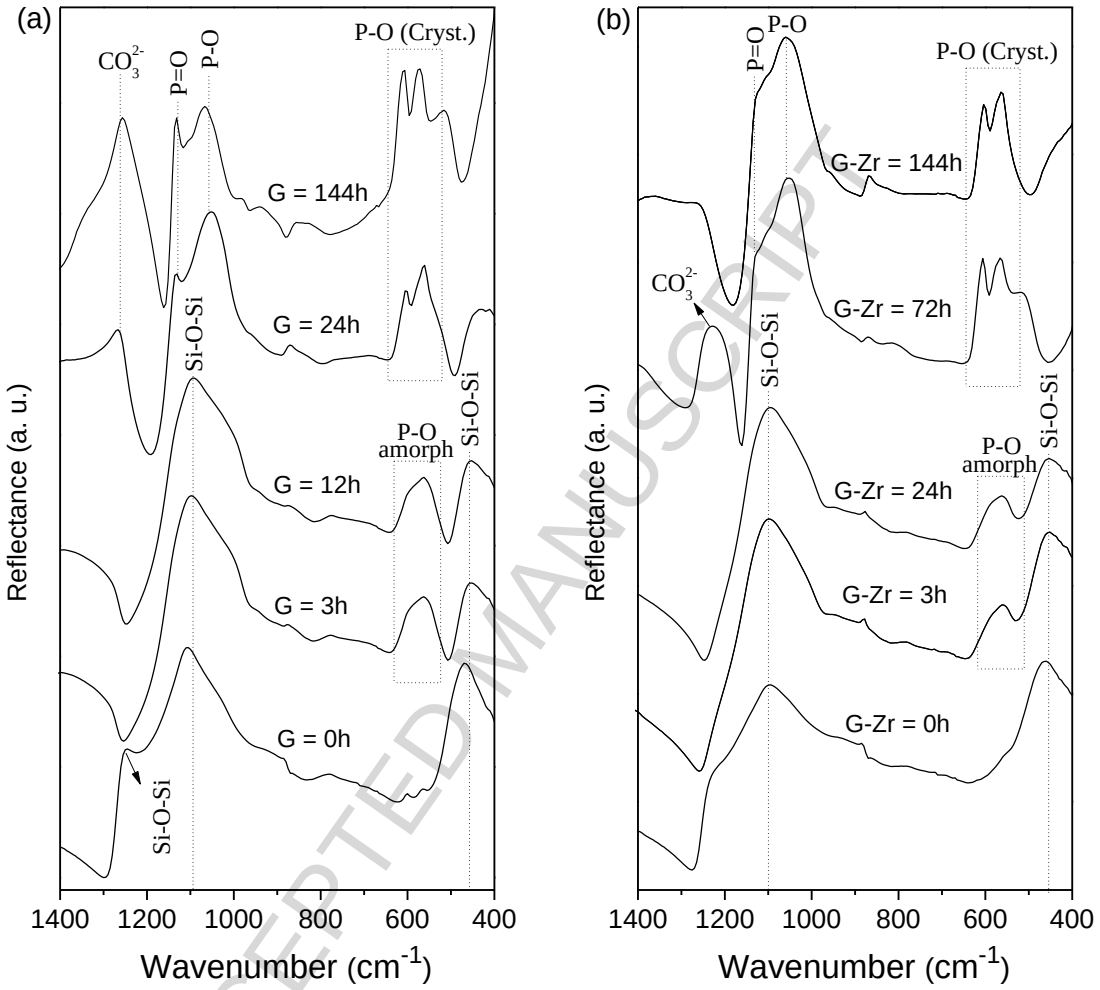

Figure 6. FTIR spectra of samples G (a) and G-Zr (b) before and after soaking in SBF at different testing times.

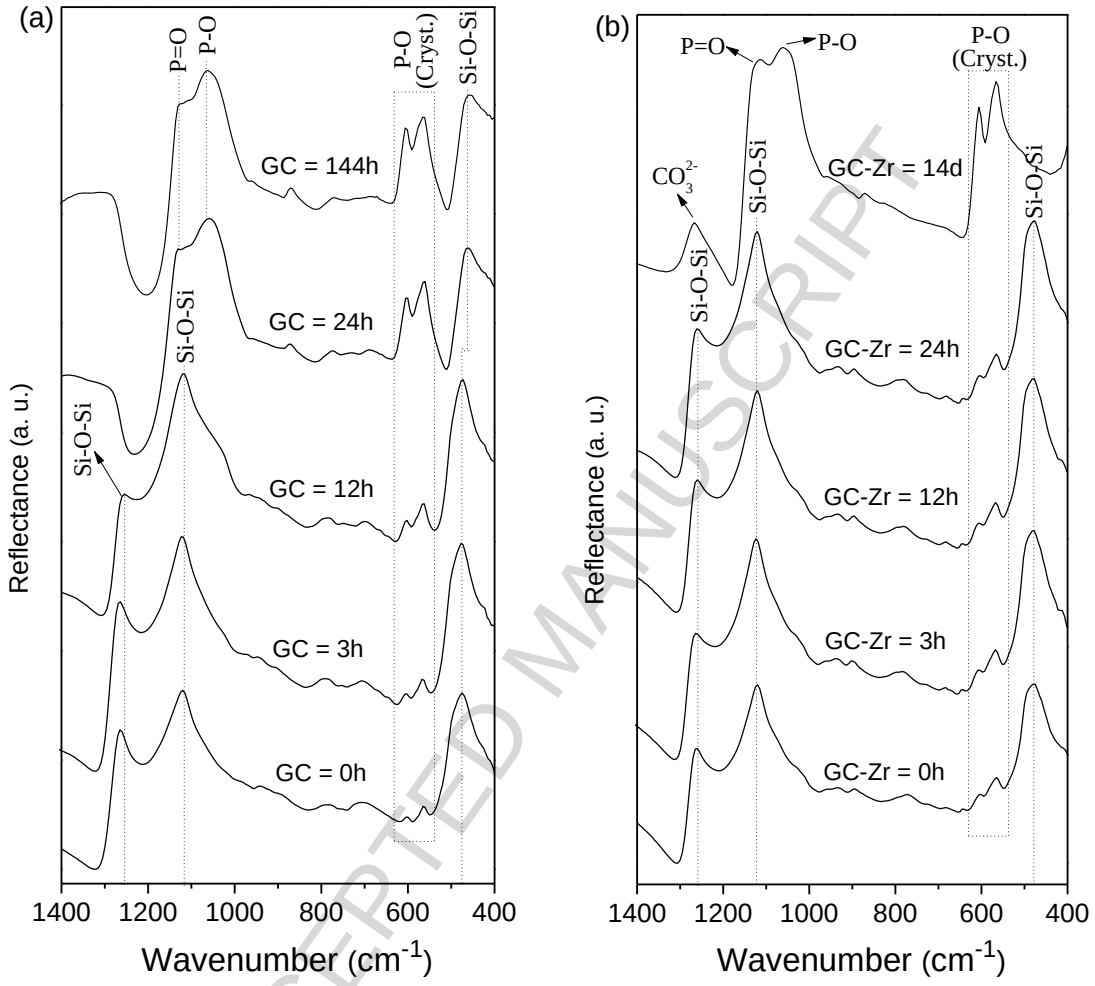

Figure 7. FTIR spectra of samples GC (a) and GC-Zr (b) before and after soaking in SBF at different testing times.

The FTIR spectra from the surfaces of the glass-ceramics before exposure to SBF and after 3 h and 12 h (Fig. 7 a-b) demonstrate three broad bands at approximately 1260 cm^{-1}, 1120 cm^{-1} and 470 cm^{-1}, which can be attributed to the vibration of the chemical bonds in the crystalline phases and Si–O–Si bond vibration. Additionally, two identified peaks at wavenumbers 605 cm^{-1} and 560 cm^{-1} can be ascribed to the deformation modes of the P–O bond in such phosphate-like phases as hydroxyapatite. Because the HCA formation on the glass-ceramic surfaces was not observed by SEM after 3 h and 12 h, these two vibration bands could be attributed to crystalline hydroxyapatite in the polycrystal matrix, which was confirmed by the

XRD results (Fig. 2). This observation suggests that the presence of P-O vibration band in the FTIR spectra is due to the HA crystals in the material and not HA formation on the surface.

After increasing the testing time to 24 h and 144 h, HCA covered the surface of the Zr-free glass-ceramic (GC-24 and GC-144), and a new spectrum was detected by FTIR that displayed the typical HCA bands located near 1130 cm^{-1}, 1060 cm^{-1}, 605 cm^{-1} and 560 cm^{-1}. However, in the glass-ceramic containing zirconia (Fig. 7-b), HCA vibration bands appear only after 14 days of exposure to SBF. However, it should be noted that HCA formation was previously confirmed via SEM after 24 h (Fig. 4). It was observed that HCA grows inside the pores and does not fully cover the surface after this time. Therefore, the FTIR spectra reflected from the surface could be primarily related to the glass-ceramic matrix rather than superficial HCA. Hence, it can be observed that HCA covers the surface of the zirconia containing glass-ceramic after 14 days.

3.3.2. pH variations and ion release during soaking in SBF

Variations in pH versus soaking time in SBF for all samples are illustrated in Figure 8. Glasses G and G-Zr present similar trends in pH variation; i.e., the pH increases constantly up to the 48 h and remains nearly constant until the last testing time of 96 h. For the GC sample, the pH range maintained a tendency to increase throughout the test, whereas for the sample GC-Zr, the pH increased only slightly up to 48 h and subsequently remained practically constant. Therefore, by comparing the pH variation for all samples during the *in vitro* bioactivity test, we can observe that the most abrupt change occurred for the sample G in the first few hours. Additionally, the lowest pH variation was observed for the sample GC-Zr, indicating that the solubility of this sample is lower than that of the others because the pH variation has a direct relationship with calcium release from the sample to the media.

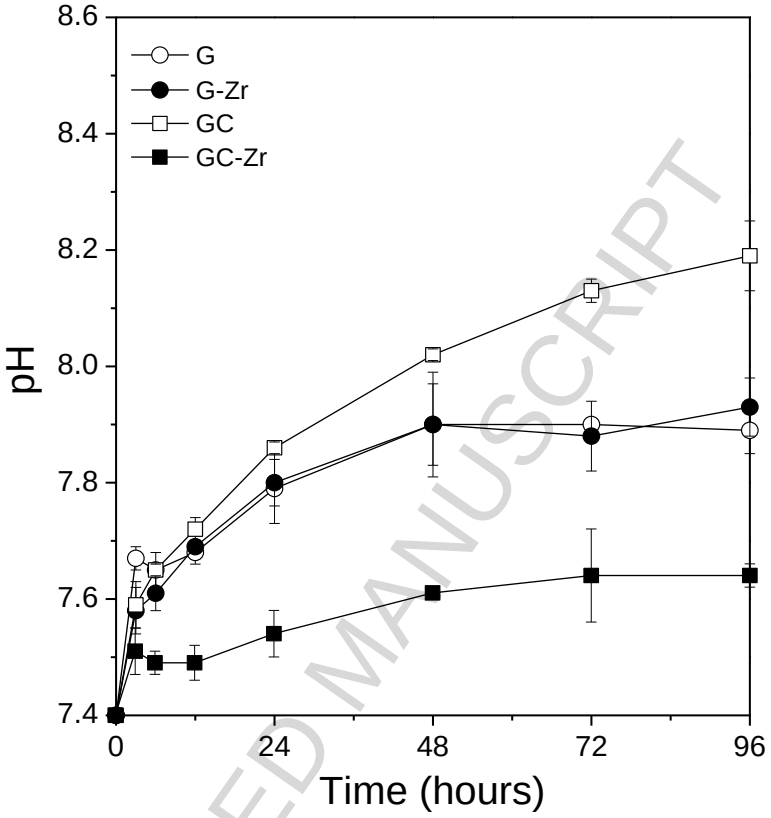

Figure 8. Variations in pH versus soaking time in SBF.

The ionic concentration of calcium, phosphorus, silicon and zirconium in the SBF after different testing times is illustrated in Figures 9 (a-d), respectively. The Ca concentration follows the pH variation. Although the average value for the Ca concentration in SBF for sample G-Zr was higher than that for sample G, the deviations overlap. Therefore, these two samples show quite similar amounts of Ca concentration during the test and result in nearly the same pH variations. In sample GC, the Ca concentration increases gradually up to the end of the test, which justifies the higher pH variation observed in Figure 8. However, GC-Zr shows a minimum concentration of Ca in SBF that remains practically constant, in agreement with the lower pH variation compared with that of other samples. The plots for phosphorous concentration show a common feature, i.e., all samples show an initial abrupt decrease in phosphorous concentration followed by a gradual decrease up to the end of the testing time. Phosphorous is released into solution and subsequently migrates to the sample surface to form a HCA layer. It appears that the rate of HCA formation is higher than the rate of phosphorous release, resulting in the decrease of P content in SBF during the *in vitro* test. The concentration of phosphorous in SBF after different

testing times for sample GC-Zr is lower than that of the other samples and remains unchanged. This observation is due to the low solubility of this sample, which imposes a minimum release of phosphorous from the sample and maximum absorption by HCA that consumes nearly all of the P in the SBF. The Si content in the SBF increases rapidly in the first 24 h and subsequently gradually increases with time. Sample GC releases the highest amount of Si, whereas sample GC-Zr presents the lowest values. The amounts of Zr release from samples G-Zr and GC-Zr are quite low and become constant after 24 h.

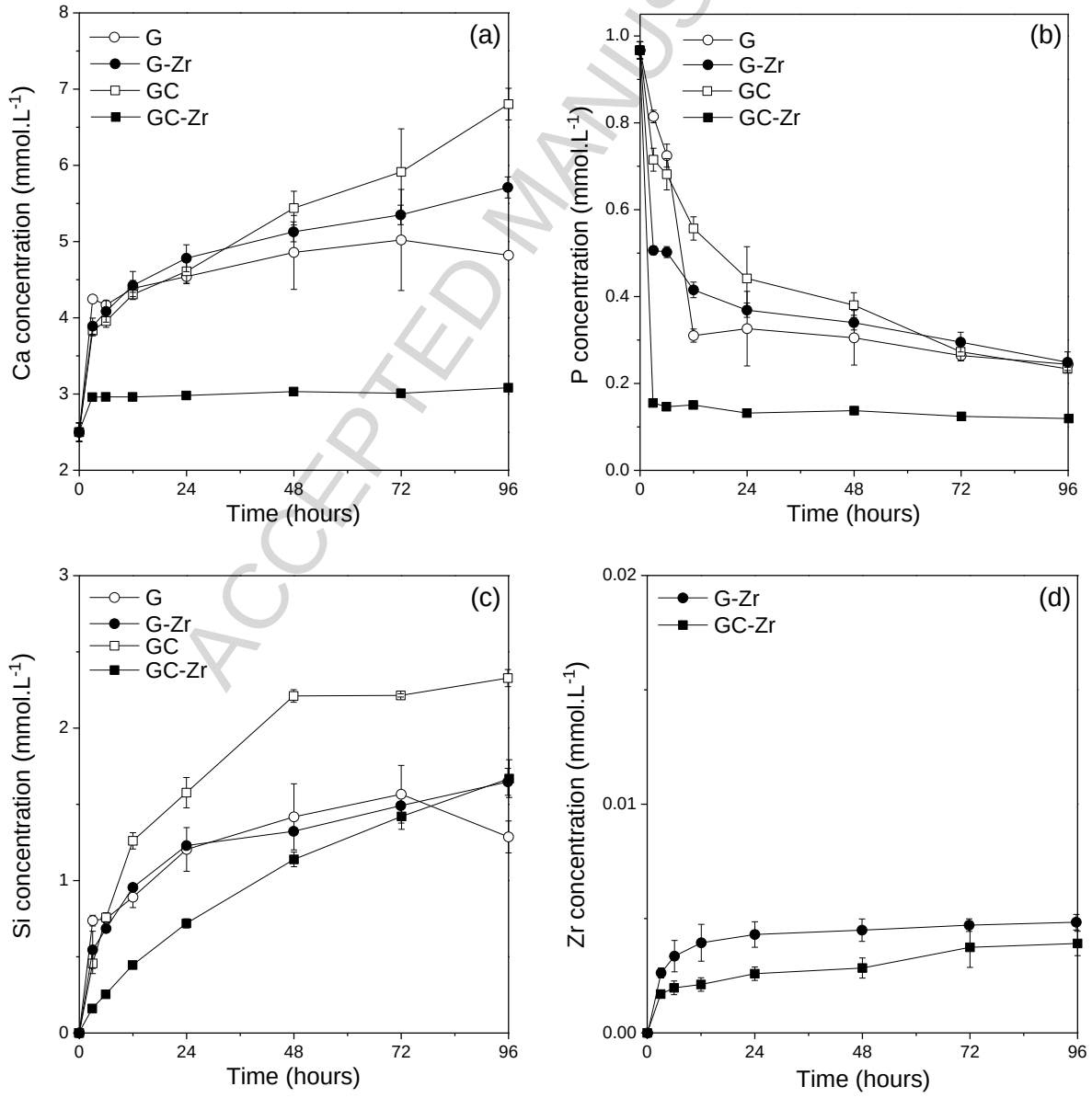

Figure 9. Ion concentration of (a) Ca, (b) P, (c) Si and (d) Zr in SBF after various soaking times.

It should be noted that Ca and P release are controlled by two opposite processes: (a) leaching from the sample to the SBF increases the calcium, silicon and phosphorous concentrations, and (b) growth of the calcium phosphate layer decreases the calcium and phosphorus concentrations in the solution [2,7,9]. In this study, the rate of Ca release is higher than the rate of formation of HCA (except for sample GC-Zr), which results in an increased ionic concentration of this element during the test. However, the phosphorous concentration in the SBF decreases with time due to the greater rate of HCA formation than that of phosphorous release from the sample. Keeping in mind that the pH and its variation is a direct consequence of ions released from the sample to the SBF solution, it can be stated that sample GC shows the highest solubility, and the GC-Zr shows the lowest solubility, thus maintaining a more stable environment.

Therefore, it appears that ZrO_2 addition to the base glass (Sample G) has only a minor influence on the pH variation as well as the dissolution of Ca, P and Si, whereas crystallization changes the behavior of these glasses. After crystallization, glass G converts to polycrystal GC (apatite-wollastonite) which shows high solubility. However, crystallization of G-Zr to GC-Zr (apatite-wollastonite-zirconia) significantly reduces the solubility. The highest amount of Ca and Si released from the sample GC can be attributed to the dissolution of the crystalline wollastonite phase ($CaSiO_3$), which has been reported as a biodegradable and soluble material [49,50,52]. However, crystallization of G-Zr to GC-Zr remarkably suppresses the release of Ca and P, whereas the Si release maintains an increasing trend. The trend for Si release in GC-Zr may be related to wollastonite dissolution. In this case, the Ca released by wollastonite dissolution and the P from the SBF solution are consumed to form HCA on the GC-Zr surface. For this reason, the formation of HCA on the surface of GC-Zr can be still observed. Furthermore, the results show that crystallization of ZrO_2 suppresses the release of Ca. This observation can be explained if calcium enters the structure of ZrO_2 to form a solid solution. This phenomenon also was observed by Kasuga *et al.* [30,31], who sintered bioactive glass powder reinforced with zirconia particles; these researchers additionally detected Ca in the zirconia particles and showed that calcium has great tendency to leave the parent glass and form a solid solution with zirconia [30,31]. A similar phenomenon is imaginable for this study, and thus zirconia may accommodate

Ca in its structure. Because zirconia has a low solubility in aqueous environment [27,51], it will simultaneously reduce the dissolution of Ca. The remaining amount of Ca released from the residual glass and wollastonite activates the bioactivity of this sample. It appears that the rate of Ca release is equal to its consumption in HCA formation. Therefore, GC-Zr remains bioactive and shows HCA formation even if it has a low level of Ca dissolution. This phenomenon may be responsible for the HCA formation in sample GC-Zr immediately after 24 h.

3.4. Cell Proliferation

As shown in Figure 10, osteoblast-like MG-63 cells cultured on the samples G, G-Zr, GC and GC-Zr showed increasing proliferation throughout the time of analysis, indicating that all samples are biocompatible, support cell proliferation, and thus do not show *in vitro* toxicity. As Lee *et. al.* [53] reported that cell culture medium can be an alternative to simulated body fluid (SBF); we assumed a similar time frame for HCA formation under cell culture conditions. At 1 day and 3 days after cell seeding, all samples reached nearly the same values of cell proliferation. This observation could indicate a characteristic behavior of these cells during the initial hours after cell seeding. Because we began with a relatively low cell density (i.e., 1×10^4 per well) that was calculated to ensure continuous growth over 18 days, osteoblasts were present in a relatively low number at three days, and thus, significant changes could not be detected. However, after 6 days (144 h), when the osteoblasts had proliferated more extensively, the glass-ceramic GC-Zr exhibited the highest cell viability values in comparison with those of G, G-Zr and GC samples. This observation can be attributed to the pH changes that occurred in different ways for different samples in the environments into which osteoblasts were inserted. As previously discussed, GC-Zr represented the lowest pH trend compared with those of other samples during *in vitro* bioactive test (Figure 8). The pH stability, which must be established at approximately 7.2 to 7.4, is a crucial factor for cell metabolism and thus for cell proliferation [54]. It is worthy of note that the cell culture medium was changed every two days, but the ion release could still be sufficiently high to induce pH changes, primarily in the initial days of the cell proliferation experiments.

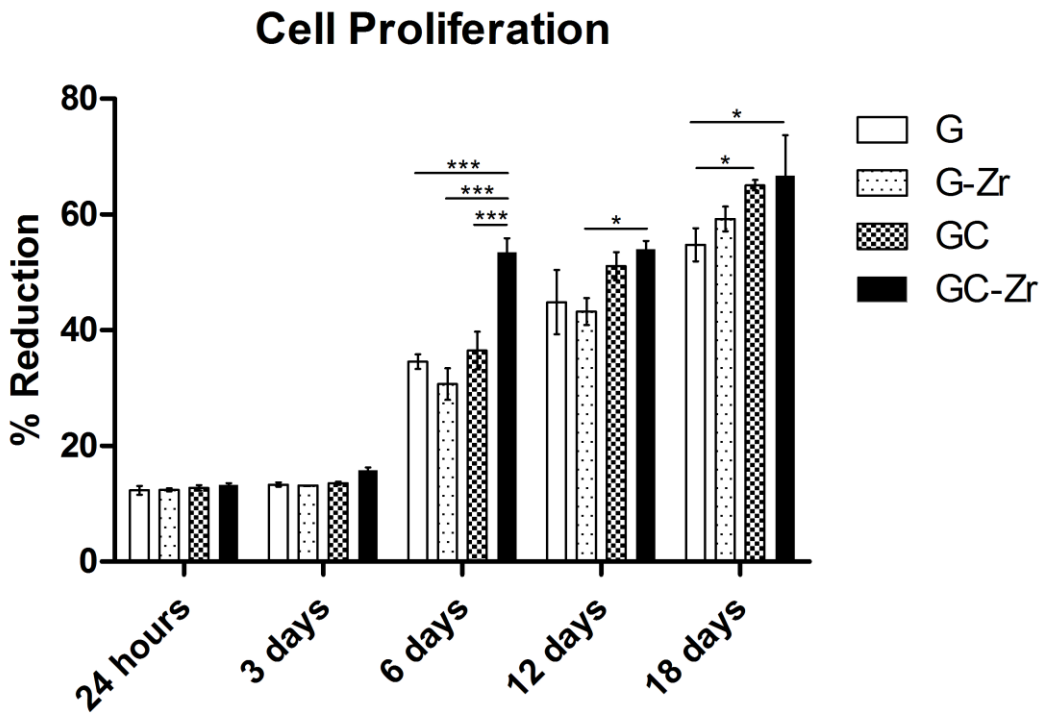

Figure 10. Effects on the viability of MG-63 cultivated for 18 days on G, G-Zr, GC an GC-Zr samples. The higher the percentage of reduction of AlamarBlue® (% reduced), the greater the amount of viable cells will be. Each column represents the mean ± S.E.M. (Standard Error of the Mean) for triplicates. *p<0.05. ***p<0.001.

Once the HCA fully covers the sample surfaces, ion release does not experience abrupt variations. Consequently, over 12 days of cell culture, the pH of the sample wells is more stable, and osteoblasts cultivated with G, G-Zr and GC proliferate in a manner similar to that of sample GC-Zr. Moreover, the difference in the cell proliferation rate between GC-Zr and G-Zr can be attributed to this period of stabilization of the cell culture environment. After 18 days of osteoblast culture, cell proliferation on G-Zr reached (statistically) the same values as those of the other samples, likely due to the pH stabilization. It is important to note that at this test time, the surfaces of all samples were completely covered by HCA (stabilized surface), as shown by the *in vitro* bioactivity assays, although the mean values recorded in the test were different.

Despite the higher pH variation in SBF observed for the sample GC compared with those of the other samples, osteoblast proliferation reached the level of GC-Zr at the final testing times.

After ion release became stagnant because the HCA fully covered the sample surfaces in the SBF, the environment surrounding the GC samples became more stable, and the cell proliferation rate increased. Moreover, GC samples presented a higher and more stable Si release after 48 h of testing time (Figure 9 (c)). According to Reffitt *et al.* [55], Si release enhances osteoblast (MG-63) proliferation, differentiation, and collagen production under *in vitro* conditions. In addition, Han *et al.* [56] observed that the Si ions significantly enhance the proliferation of bone marrow stromal cells. Consequently, superior and continuous Si release of GC samples could contribute to osteoblast proliferation.

It is important to mention that other features of these samples can affect cell proliferation. Further studies, such as cell adhesion and reverse transcriptase Polymerase Chain Reaction (rt-PCR), are necessary to understand how HCA surface coverage and Ca, P and Zr release can affect cell adhesion and gene expression, respectively. These experiments could better elucidate the biological interaction between osteoblasts and these bioactive glasses and polycrystals. In addition, a complementary cell proliferation test carried out from 24 h to 6 days and measured every 24 h could be used to detect significant differences that may be related to the pH or ions release of the different samples.

4. Conclusions

In this study, 10 mol% zirconia was successfully incorporated in a bioactive composition via a simple sol-gel method. Both glass and glass-ceramic containing Zr are bioactive. However, Zr postpones the *in vitro* formation of HCA on the glass surface for a few days. Therefore, dissolved Zr in the glass structure retards HCA formation and could be used to control its formation rate. For the glass-ceramic containing ZrO_2 crystals, HCA was observed just after one day. It appears that Ca leaching from the residual glass and wollastonite dissolution encourages the precipitation of HCA.

Cell proliferation analysis indicated that the glass-ceramic containing zirconia shows significantly higher osteoblast propagation in comparison with that of the other samples in the first hours of the test. Addition of zirconia to this system decreases the solubility of the samples and consequently diminishes the variation of the pH media containing the cells. In addition, we

demonstrated that all samples are biocompatible, support cell proliferation, and show no *in vitro* toxicity, making these materials potential candidates for radiopaque bone graft substitutes and bone cements.

5. Acknowledgements

The authors are grateful to the Iran National Science Foundation (INFS, # 92007700) and São Paulo Research Foundation (FAPESP), Brazil (# 2013/07793-6) for financial support of this research project. We also acknowledge Conselho Nacional de Desenvolvimento Científico e Tecnológico (CNPq), Brazil, and The World Academy of Sciences (TWAS) for funding a Sandwich *PhD* fellowship for Maziar Montazerian (# 302976/2013-2).

6. References

[1] Li, R., **Sol-gel processing of bioactive glass powders**. PhD Dissertation, University of Florida, 1991.

[2] Pereira, M. M., Clark, A. E. and Hench, L. L., **Calcium phosphate formation on sol-gel-derived bioactive glasses *in vitro*.** J. Biomed. Mater. Res., 1994, 28[6], 693-698.

[3] Pereira, M. M., Clark, A. E. and Hench, L. L., **Effect of texture on the rate of hydroxyapatite formation on gel-silica surface.** J. Am. Ceram. Soc., 1995, 78[9], 2463-2468.

[4] Jones, J. R., **Review of bioactive glass: from Hench to hybrids.** Acta Biomaterialia, 2013, 9[1], 4457-4486.

[5] Arcos, D. and Vallet-Regí, M., **Review: Sol-gel silica-based biomaterials and bone tissue regeneration.** Acta Biomaterialia, 2010, 6, 2874-2888.

[6] Erol-Taygun, M., Zheng, K. and Boccaccini, A. R., **Nanoscale bioactive glass in medical application.** Int. J. App. Glass Science, 2013, 4[2], 136-148.

[7] Izquier-Barba, I., Salinas, A. J. and Vallet-Regí, M., **Bioactive glasses: from macro to nano.** Int. J. App. Glass Science, 2013, 4[2], 149-161.

[8] Vallet-Regí, M., Salinas, A. J. and Arcos, D., **From the bioactive glasses to the star gels.** J. Mater. Sci.: Mater. Med., 2006, 17, 1011-1017.

[9] Vallet-Regí, M., **Revisiting ceramics for medical applications.** J. Chem. Soc., 2006, 5211-5220.

[10] Roman, J., Padilla, S. and Vallet-Regí, M., **Sol-gel glasses as precursors of bioactive glass-ceramics.** Chem. Mater., 2003, 15, 798-806.

[11] Siqueira, R. L. and Zanotto, E. D., **The influence of phosphorus precursors on the synthesis and bioactivity of SiO_2–CaO–P_2O_5 sol–gel glasses and glass–ceramics.** J. Mater. Sci.: Mater. Med., 2013, 24, 365-379.

[12] Siqueira, R. L., Peitl, O. and Zanotto, E. D., **Gel-derived SiO_2–CaO–Na_2O–P_2O_5 bioactive powders: synthesis and *in vitro* bioactivity**. Mater. Sci. Eng. C, 2011, 31[5], 983-991.

[13] Siqueira, R. L. and Zanotto, E. D., **Facile route to obtain a highly bioactive SiO_2–CaO–Na_2O–P_2O_5 crystalline powder.** Mater. Sci. Eng. C, 2011, 31[12], 1791-1799.

[14] Saboori, A., Rabiee, M., Moztarzadeh, F., Sheikhi, M., Tahriri, M. and Karimi, M., Synthesis, **Characterization and *in vitro* bioactivity of sol-gel-derived SiO_2–CaO–P_2O_5–MgO bioglass.** J. Mater. Sci. Eng. C, 2009, 29, 335-340.

[15] Ma, J., Chen, C. Z., Wang, D. G. and Shi, J. Z., **Textural and structural studies of sol-gel derived SiO_2–CaO–P_2O_5–MgO glasses by substitution of MgO for CaO.** J. Mater. Sci. Eng. C, 2010, 30, 886-890.

[16] Oki, A., Parveen, B., Hossain, S., Adeniji, S. and Donahue, H., **Preparation and *in vitro* bioactivity of zinc containing sol-gel-derived bioglass materials.** J. Biomed. Mater. Res. Part A, 2004, 69[2], 216–221.

[17] Balamurugan, A., Balossier, G., Kannan, S., Michel, J., Rebelo, A. H. S. and Ferreira, J .M. F., **Development and *in vitro* characterization of sol-gel derived CaO–P_2O_5–SiO_2–ZnO bioglass.** Acta Biomaterialia, 2007, 3, 255-262.

[18] Balamurugan, A., Balossier, G., Laurent-Maquin, D., Pina, S., Rebelo, A. H. S., Faure, J. and Ferreira, J. M. F., **An *in vitro* biological and anti-bacterial study on a sol-gel derived silver-incorporated bioglass system.** Dental Materials, 2008, 24, 1343-1351.

[19] Chatzistavrou, X., Fenno, J. C., Faulk, D., Badylak, S., Kasuga, T., Boccaccini, A. R. and Papagerakis, P., **Fabrication and characterization of bioactive and antibacterial composites for dental applications.** Acta Biomaterialia, 2014, 10[8], 3723–3732.

[20] Hesaraki, S., Gholami, M., Vazehrad, S. and Shahrabi, S., **The effect of Sr concentration on bioactivity and biocompatibility of sol–gel derived glasses based on CaO–SrO–SiO_2–P_2O_5 quaternary system.** J. Mater. Sci. Eng. C, 2010, 30, 383-390.

[21] Salinas, A.J., Shruti, S., Malavasi, G., Menabue, L. and Vallet-Regí, M., **Substitutions of cerium, gallium and zinc in ordered mesoporous bioactive glasses.** Acta Biomaterialia, 2011, 7[9], 3452–3458.

[22] Li, H. C, Wang, D. G., Hu, J. H. and Chen, C. Z., **Crystallization, mechanical properties and *in vitro* bioactivity of sol–gel derived Na_2O–CaO–SiO_2–P_2O_5 glass–ceramics by partial substitution of CaF_2 for CaO.** Sol-Gel Sci. Technol., 2013, 67, 56–65.

[23] Li, H. C, Wang, D. G., Hu, J. H. and Chen, C. Z., **Effect of the partial substitution of K_2O, MgO, B_2O_3 for CaO on crystallization, structure and properties of Na_2O–CaO–SiO_2–P_2O_5 system glass-ceramic.** Materials Letters, 2013, 106, 373-376.

[24] Roberto, W. S., Pereira, M. M. and Campos, T. P. R., **Analysis of bioactive glasses obtained by sol-gel processing for radioactive implants.** Mater. Res., 2003, 6[2], 123-127.

[25] Łączka, M., Cholewa-Kowalska, K., Łączka-Osyczka, A., Tworzydlo, M. and Turyna, B., **Gel-derived materials of a CaO–P_2O_5–SiO_2 system modified by boron, sodium, magnesium, aluminum, and fluorine compounds.** J. Biomed. Mater. Res., 2000, 52, 601-612.

[26] Pawlik, J., Widziołek, M., Cholewa-Kowalska, K., Ła□czka, M. and Osyczka, A. M**. New sol-gel bioactive glass and titania composites with enhanced physico-chemical and biological properties.** J. Biomed. Mater. Res. Part A, 2014, 102[7], 2383-2394.

[27] Afzal, A., **Implantable zirconia bioceramics for bone repair and replacement: A chronological review.** Mater. Express, 2014, 4[1], 1-12.

[28] Nothdurft, F. P. and Pospiech, P. R., **Clinical evaluation of pulpless teeth restored with conventionally cemented zirconia posts: A pilot study**. J. Prosthet. Dent., 2006, 95[4], 311-314.

[29] Schweiger, M., Frank, M., Clausbruch, C. V., Höland, W. and Rheinberger, V., **Microstructure and properties of a composite system for dental applications composed of glass–ceramics in the SiO_2–LiO_2–ZrO_2–P_2O_5 system and ZrO_2-ceramic (TZP).** J. Mater. Sci., 1999, 34, 4563-4572.

[30] Kasuga, T., Yoshida, M., Ikushima, A. J., Tuchiya, M. and Kusakari, H., **Bioactivity of zirconia-toughened glass-ceramics.** J. Am. Ceram. Soc., 1992, 75[7], 1884-1888.

[31] Kasuga, T., Nakajima, K., Uno, T. and Yoshida, M., **Preparation of zirconia-toughened bioactive glass-ceramic composite sinter-hot isostatic pressing.** J. Am. Ceram. Soc., 1992, 75, 1103-1107.

[32] Montazerian, M., Alizadeh, P. and Eftekhari Yekta, B., **Pressureless sintering and mechanical properties of mica glass–ceramic/Y-PSZ composite.** J. Eur. Ceram. Soc., 2008, 28, 2687-2692.

[33] Montazerian, M., Alizadeh, P. and Eftekhari Yekta, B., **Processing and properties of a mica–apatite glass–ceramic reinforced with Y-PSZ particles**. J. Eur. Ceram. Soc., 2008, 28, 2693-2699.

[34] Ghaffari, M., Alizadeh, P. And Rahimipour, M. R., **Sintering behavior and mechanical properties of mica-diopside glass–ceramic composites reinforced by nano and micro-sized zirconia particles.** J. Non-Cryst. Solids, 2012, 358[23], 3304–3311.

[35] Verné, E., Defilippi, R., Carl, G., Vitale Brovarone, C. and Appendino, P., **Viscous flow sintering of bioactive glass-ceramic composites toughened by zirconia particles.** J. Eur. Ceram. Soc., 2003, 23, 675-683.

[36] Mondal, D., So-Ra, S. and Lee, B. T., **Fabrication and characterization of ZrO_2–CaO–P_2O_5–Na_2O–SiO_2 bioactive glass ceramics.** J. Mater. Sci., 2013, 48[5], 1863-1872.

[37] Zhu, Y., Zhang, Y., Wu, C., Fang, Y., Yang, J. and Wang, S., **The effect of zirconium incorporation on the physiochemical and biological properties of mesoporous bioactive glasses scaffolds.** Microporous and Mesoporous materials, 2011, 143, 311-319.

[38] Persson, C., Unosson, E., Ajaxon, I., Engstrand, J., Engqvist, H. and Xia, W., **Nano grain sized zirconia–silica glass-ceramics for dental applications,** Journal of the European Ceramic Society. 2012, 32[16], 4105-4110.

[39] Ananth, K. P., Suganya, S., Mangalaraj, D., Ferreira, J.M.F. and Balamurugan, A., **Electrophoretic bilayer deposition of zirconia and reinforced bioglass system on Ti6Al4V for implant applications: An *in vitro* investigation.** J. Mater. Sci. Eng. C, 2013, 33, 4160-4166.

[40] Tallia, F., Gallo, M., Pontiroli, L., Baino, F., Fiorilli, S., Onida, B., Anselmetti, G. C., Manca, A. and Vitale-Brovarone, C., **Zirconia-containing radiopaque mesoporous bioactive glasses.** Materials Letters, 2014, 130, 281–284.

[41] Vitale-Brovarone, C., Verné, E., Bergui, M., Onida, B., Baino, F., Miola, M. et al. **Injectable osteoinductive bone cements.** World Patent Application, WO 2011141889 A1.

[42] Kokubo, T. and Takadama, H., **How useful is SBF in predicting *in vivo* bone bioactivity?** Biomaterials, 2006, 27, 2907-2915.

[43] Hamid, R., Rotshteyn, Y., Rabadi, L., Parikh, R. and Bullock, P., **Comparison of alamar blue and MTT assays for high through-put screening.** Toxicol In Vitro, 2004, 18[5], 703-710.

[44] AlamarBlue® Technical Datasheet. AbD Serotec Endeavor House, Langford Lane, Kidlington, Oxford, UK Corpright MorphoSys UK Ltd, 2008.

[45] Krimm, S. and Tobolsky, A. V., **Quantitative X-ray studies of order in amorphous and crystalline polymers. Quantitative X-ray determination of crystallinity in polyethylene.** J. Polym. Sci., 1951, 7, 57-76.

[46] Padilla, S., Román, J., Carenas, A. and Vallet-Regí, M., **The influence of the phosphorus content on the bioactivity of sol-gel glass ceramics**. Biomaterials, 2005, 26, 475-483.

[47] Vallet-Regí, M., Román, J., Padilla, S., Doadrio, J. C. and Gil, F. J., **Bioactivity and mechanical properties of SiO_2−CaO−P_2O_5 glass-ceramics.** J. Mater. Chem. 2005, 15, 1353-1359.

[48] Manda, M., Goudouri, O., Papadopoulou, L., Kantiranis, N., Christofilos, D., Triantafyllidis, K., Chrissafis, K., Paraskevopoulos, K. M. and Koidis, P., **The effect of high tempered firing cycle on the bioactive behavior of sol–gel derived dental porcelain modified by bioactive glass.** J. Sol-Gel Sci. Technol., 2012, 63, 481–494.

[49] Ma, J., Chen, C.Z., Wang, D.G., Meng, X.G. and Shi, J.Z., **Influence of the sintering temperature on the structural feature and bioactivity of sol–gel derived SiO_2–CaO–P_2O_5 bioglass.** Ceramics International, 2010, 36[6], 1911-1916.

[50] Ni, S. Y., Chang, J. and Chou, L., **A novel bioactive porous $CaSiO_3$ scaffold for bone tissue engineering.** J. Biomed. Mater. Res. Part A, 2006, 76, 196-205.

[51] Hench, L. L., **Bioceramics.** J. Am. Ceram. Soc., 1998, 81, 1705-1728.

[52] Hazar, A. B. Y., **Preparation and *in vitro* bioactivity of $CaSiO_3$ powders.** Ceramics International, 2007, 33[4], 687-692.

[53] Lee, J. T. Y., Leng, Y., Chow, K. L., Ren, F., Ge, X., Wang, K. and Lu, X., **Cell culture medium as an alternative to conventional simulated body fluid**. Acta Biomaterialia, 2011, 7[6], 2615-2622.

[54] Alberts, B., Bray, D., Lewis, J., Raff, M., Roberts, K. and Watson, J. D., **Molecular Biology of the Cell.** 4th edition, New York, Garland Publishing, 2003.

[55] Reffitt, D. M., Ogston, N., Jugdaohsingh, R., Cheung, H. F., Evans B. A., Thompson, R. P., Powell, J. J. and Hampson, G. N., **Orthosilicic acid stimulates collagen type 1 synthesis and osteoblastic differentiation in human osteoblast-like cells *in vitro*.** Bone, 2003, 32[2], 127-135.

[56] Han, P., Wu, C. and Xiao, Y., **The effect of silicate ions on proliferation, osteogenic differentiation and cell signaling pathways (WNT and SHH) of bone marrow stromal cells**. Biomaterials Science, 2013, 1, 379-392.

Highlights

- A simple sol-gel route was used to synthesize a bioactive $CaO-P_2O_5-SiO_2-ZrO_2$ glass.
- By heat treatment, the glass converted to apatite-wollastonite-zirconia materials.
- HCA formed more rapidly on the crystalline powder surface than on the glass.
- The synthesized powders are bioactive and encourage bone cell proliferation.
- These powders are potential candidates for radiopaque bone grafts and bone cements.